Discovery of Doubly Magic ^{48}Ni

B. Blank, M. Chartier, S. Czajkowski, J. Giovinazzo, M. S. Pravikoff, and J.-C. Thomas
CEN Bordeaux-Gradignan, Le Haut-Vigneau, F-33175 Gradignan Cedex, France

G. de France, F. de Oliveira Santos, and M. Lewitowicz
Grand Accélérateur National d'Ions Lourds, B.P. 5027, F-14076 Caen Cedex, France

C. Borcea
IAP, P.O. Box MG6, Bucharest-Magurele, Romania

R. Grzywacz,* Z. Janas, and M. Pfützner
Institute of Experimental Physics, University of Warsaw, PL-00-681 Warsaw, Hoza 69, Poland
(Received 20 October 1999)

In an experiment at the SISSI/LISE3 facility of GANIL, we used the projectile fragmentation of a primary $^{58}Ni^{26+}$ beam at 74.5 MeV/nucleon with an average current of 3 μA on a natural nickel target to produce very neutron-deficient isotopes. In a 10-day experiment, 287 ^{42}Cr isotopes, 53 ^{45}Fe isotopes, 106 ^{49}Ni isotopes, and 4 ^{48}Ni isotopes were unambiguously identified. The doubly magic nucleus ^{48}Ni, observed for the first time, is the most proton-rich isotope ever identified with an isospin projection $T_z = -4$. It is probably the last doubly magic nucleus with "classical" shell closures accessible for present-day facilities. Its observation allows us to deduce a lower limit for the half-life of ^{48}Ni of 0.5 μs.

PACS numbers: 27.40.+z, 21.10.Dr, 23.50.+z, 25.70.Mn

Doubly magic nuclei have a magic attraction for nuclear physicists. These nuclei enabled them to interpret many properties of nuclei. They are spherical and exhibit a remarkable stability compared to neighboring isotopes. However, one of the questions of current interest is whether or not the role of the magic numbers, well established along the valley of stability, remains important when an extreme excess of protons or neutrons is present in a nucleus. In fact, lighter naturally occurring isotopes have roughly the same number of protons and neutrons. Thus the lightest stable isotope of the element nickel is ^{58}Ni with 28 protons and 30 neutrons, while ^{57}Ni is already unstable and decays by β^+ emission. The excess of protons or neutrons in a nucleus is characterized by the isospin-projection quantum number T_z which is half the difference between neutron and proton numbers. The most negative value for T_z is expected to occur for ^{48}Ni.

The recent observation of doubly magic ^{100}Sn [1,2] and ^{78}Ni [3] showed that projectile fragmentation is most probably the route to ^{48}Ni, and the question about its stability attracted the attention of experimentalists as well as of theorists [4–8]. The special interest of this nucleus is that it is the only case of a doubly magic nucleus in the entire chart of nuclei where the mirror nucleus, ^{48}Ca, is stable against particle emission, a fact which may allow for interesting mirror symmetry studies. In addition, with ^{48}Ni, ^{56}Ni, and ^{78}Ni, nickel is most probably the only element possessing three doubly magic nuclei. Furthermore, together with ^{45}Fe, ^{48}Ni is the prime candidate for the yet unobserved two-proton radioactivity, the emission of ^{2}He from the ground state of an isotope [4–8]. If one excludes the superheavy elements, where the magic numbers are not known experimentally, ^{48}Ni is also predicted to be the last doubly magic nucleus possessing shell closures known from spherical nuclei which is accessible with present-day techniques.

The search for doubly magic ^{48}Ni started with the advent of powerful projectile-fragmentation facilities. Thus, ^{51,52}Ni have been identified for the first time in 1986 [9] in an experiment at the LISE facility [10]. In this experiment, an average beam current of 50 nA corresponding to 1.5×10^{10} particles per second for the primary ^{58}Ni beam at 55 MeV/nucleon was available.

The next two steps towards ^{48}Ni were taken at the fragment separator FRS [11] at GSI. In a first experiment using the projectile fragmentation of a relativistic ^{58}Ni beam at 650 MeV/nucleon (5×10^7 particles per second) in 1993 [12], ^{50}Ni was observed with three events. At the same time, extensive production cross-section measurements were performed which enabled us for the first time to reliably predict the production cross section of proton-rich isotopes from ^{58}Ni fragmentation (see below). After an increase of the primary-beam intensity of about a factor of 10 from SIS at GSI, a second experiment [13] was carried out at the FRS using the projectile fragmentation of a primary ^{58}Ni beam at 600 MeV/nucleon to produce proton-rich isotopes. The experiment led to the discovery of ^{42}Cr, ^{45}Fe, and ^{49}Ni.

Intensive developments on the electron cyclotron resonance (ECR) ion sources at GANIL made it possible to start a search for doubly magic ^{48}Ni. In these developments, the metallic natural nickel used in the past was

 0031-9007/00/84(6)/1116(4)$15.00

replaced by nickelocene, a chemical compound which allowed us to treat nickel as a gas in the ECR ion source.

A primary beam of $^{58}Ni^{26+}$ with an average current of 3 μA corresponding to 7.2×10^{11} particles per second was accelerated by the GANIL cyclotrons to an energy of 74.5 MeV/nucleon. This beam impinged on a natural nickel target of thickness 230.6 mg/cm^2 followed by a 2.7 mg/cm^2 carbon stripper foil, both installed on a rotating wheel between the two superconducting solenoids of the SISSI device. The secondary beams ($B\rho_1 =$ 1.7323 T m) were transported through the Alpha spectrometer to the LISE3 separator [10]. At the intermediate focal plane of LISE3, a shaped beryllium degrader (10.36 mg/cm^2) in conjunction with the second dipole stage ($B\rho_2 =$ 1.7000 T m) allowed for a refined selection of the fragments of interest.

At the first achromatic focal plane of LISE3, a microchannel-plate (MCP) detector was mounted to yield a timing signal for each isotope. This detector had to withstand a counting rate of about 5×10^5 particles per second. It turned out that its efficiency was about 70%. The velocity filter at the end of the LISE3 device reduced the counting rate to roughly 500 particles per second. The selected isotopes were finally implanted in a silicon-detector telescope consisting of five detectors, the first three with a thickness of 300 μm each, the fourth with a thickness of 700 μm, and the last one with a thickness of 6 mm. The first detector (active area 600 mm^2) was used for an energy-loss and a time-of-flight measurement, whereas the second detector (quadratic shape with an area of 3×3 cm^2) was position sensitive (resistive readout) and thus yielded an energy-loss and a two-dimensional position measurement with a spatial resolution of about 1 mm. The isotopes of interest were finally implanted in the third detector (600 mm^2) which measured the residual energy and yielded another timing signal. Most of the lighter or less exotic particles were stopped in the first two silicon detectors. Thus the counting rate in the implantation detector was only about 10–15 particles per second. The last two detectors served as veto detectors and had sizes of 15×40 mm^2 and of 600 mm^2.

This detection setup enabled us to measure 10 independent parameters to identify the isotopes for each implantation event: three energy signals in the first three silicon detectors, two veto signals in the fourth and the fifth detectors, positions in x and y, and three independent flight times (TOF). The TOFs were measured between the MCP detector and the first silicon detector, the first silicon detector and the cyclotron radiofrequency, as well as between the third silicon detector and the radiofrequency.

To analyze the data, the average value for each of these 10 parameters as well as its full width at half maximum (FWHM) was determined for each isotope based on the experimental observation. In order to calculate the parameters for particle-unstable isotopes not present in the spectra, interpolations and extrapolations from the measured values of neighboring nuclei were used. The expected average value for isotopes with isospin projections from $T_z = -2$ to $T_z = -9/2$ and with nuclear charges from $Z = 22$ to $Z = 29$ was calculated for each parameter. To accept an event, all parameters had to lie within a window of two FWHM. However, for the graphical representation, these cuts were applied only for parameters not represented in the spectrum. Figure 1 shows the result of this analysis as a plot of the energy loss in the first silicon detector as a function of the TOF between the MCP detector and the first silicon detector. Because of the efficiency of the MCP detector, part of the statistics is lost in this spectrum. Nevertheless, two events of ^{48}Ni are clearly observed. In particular, no background events are observed in the whole region analyzed between the unbound ^{54}Cu at the upper left end and the unbound ^{35}Ti at the lower right end. In addition, 77 events of ^{49}Ni, 29 events of ^{45}Fe, and 164 events of ^{42}Cr fulfill the stringent conditions imposed on this spectrum. Already from this spectrum we conclude therefore that the new doubly magic nucleus ^{48}Ni has been unambiguously identified.

To circumvent the lack of efficiency of the MCP detector, we analyzed the data also as a function of the energy loss in the first silicon detector and the total energy as the sum of the signals in the first three silicon detectors. For this analysis, we used the information from the MCP detector only, if it was present, i.e., if the TOF signal of this detector and the first silicon detector was above zero. The result of this analysis is shown in Fig. 2. In this spectrum, we observe four counts which we can unambiguously attribute to ^{48}Ni. The number of counts for ^{49}Ni, ^{45}Fe, and ^{42}Cr are 89, 48, and 264, respectively.

This spectrum, however, demonstrates also the importance of the MCP detector, as all background counts are events without MCP timing. In fact, we identify one background count at the positions of the unbound ^{51}Cu, ^{45}Mn, ^{42}V, and ^{41}V, whereas the other counts could be rejected

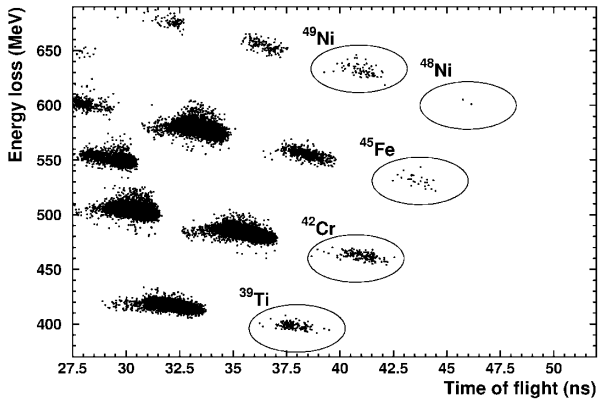

FIG. 1. Two-dimensional identification plot of energy loss in the first silicon detector versus the TOF between the MCP detector and the silicon detector. To produce this spectrum, software conditions were applied to all parameters except those represented here (see text for details). Because of the efficiency of the MCP detector, part of the events are lost in this spectrum.

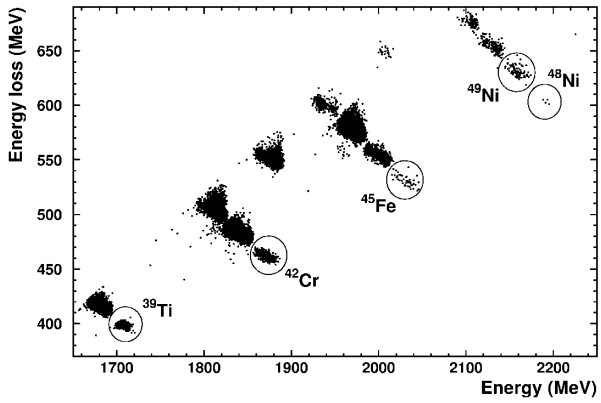

FIG. 2. Two-dimensional identification plot of energy loss in the first silicon detector versus the total energy calculated as the sum energy of the first three silicon detectors. As for Fig. 1, software conditions were applied to all parameters except those represented here (see text for details). Less exotic isotopes were cut either by software conditions or by the transmission of LISE3.

due to their wrong energy-loss/energy relation in this spectrum. However, none of these background counts are accumulated in a particular region in this energy-loss/energy matrix, like it is the case for the four ^{48}Ni events. Therefore, it seems rather unlikely that more than one of these four events is background.

From Figs. 1 and 2, we conclude that the new doubly magic nucleus ^{48}Ni has been observed for the first time. The observation of ^{49}Ni, ^{45}Fe, and ^{42}Cr confirms the results from the 1996 GSI experiment [13] where these isotopes were observed for the first time with much lower counting rates.

The number of counts of the present experiment for the four most proton-rich isotopes ^{48}Ni, ^{49}Ni, ^{45}Fe, and ^{42}Cr is given in Table I. In order to have all counts for each nucleus to calculate the production cross sections, we used three FWHM windows to determine the number of counts. To estimate their production cross section we calculated the Alpha+LISE3 transmission for these isotopes with three different simulation codes, the programs LISE [14], LIESCHEN [15], and INTENSITY [16]. The INTENSITY code has no feature to treat the velocity filter of the LISE3 separator. However, it turned out in the simulations with the two other codes that the velocity-filter transmission for the four isotopes discussed here is 100% and thus INTENSITY calculations yield the total transmission in these special cases. In Table I, we give the average transmission from the three simulations. The error is estimated from the difference of the predictions. Except for ^{42}Cr which is close to the acceptance limit of LISE3 at the intermediate focal plane, the different codes predict transmissions within a window of about 50%.

The production cross sections for ^{48}Ni, ^{49}Ni, ^{45}Fe, and ^{42}Cr in the present experiment can be deduced from this information, the ^{nat}Ni target thickness of 230.6 mg/cm^2 and a total beam dose of 4.2×10^{17} particles. These cross sections are presented in Table I. They are compared to the new EPAX formula [17], an empirical parametrization of projectile fragmentation cross sections. We find nice agreement between experimentally determined cross sections and predictions from EPAX, especially for ^{48}Ni and ^{49}Ni. However, the experimental production cross section for ^{45}Fe is more than a factor of 2 lower than expected. From the cross-section systematics measured for the fragmentation of a ^{58}Ni primary beam [12], a decrease of a factor of 2 is not expected between ^{49}Ni and ^{45}Fe. A possible explanation could be that part of the ^{45}Fe activity decays in-flight with a half-life of roughly 0.5 μs. However, we cannot exclude that the production cross section for ^{45}Fe might be smaller than expected or that the transmission calculations have a larger error. Therefore, additional information, namely, measurements of its decay as well as a measurement similar to the present experiment, but with a significantly shorter flight time, are necessary to confirm or reject this hypothesis.

^{48}Ni is predicted particle unstable by all commonly used mass models. As it is an even-Z nucleus, these models foresee that the one-proton emission is energetically forbidden and thus ^{48}Ni may decay by two-proton emission. However, the model predictions for the Q value for two-proton emission, Q_{2p}, vary between less than 1.0 MeV and more than 3.0 MeV (see Fig. 3). Using barrier-penetration calculations this gap yields partial half-lives for two-proton

TABLE I. Pertinent information concerning the production cross sections of ^{48}Ni, ^{49}Ni, ^{45}Fe, and ^{42}Cr. The first line gives the number of counts experimentally observed. The numbers given correspond to three FWHM windows for each parameter (see text). The error bars are the sum of statistical and systematic errors. The systematic errors have been determined by varying the conditions used to identify the isotopes. The transmissions in the second line are averages from three different model calculations with LISE [14], LIESCHEN [15], and INTENSITY [16]. The experimental cross sections (third line) are determined with a primary-beam dose of 4.2×10^{17} particles and a ^{nat}Ni target thickness of 230 mg/cm^2. In addition, a dead time correction of 13% is applied. Losses due to secondary reactions in target and degrader are below the 1% level and are not taken into account. The last line gives the predictions from the new EPAX parametrization [17].

	^{48}Ni	^{49}Ni	^{45}Fe	^{42}Cr
Number of counts	4 ± 2	106 ± 22	53 ± 9	287 ± 30
Transmission (%)	9.8 ± 1.2	6.9 ± 1.6	6.7 ± 0.3	0.7 ± 0.6
Cross section (pb)	0.05 ± 0.02	1.8 ± 0.6	0.9 ± 0.2	$47 \pm^{285}_{22}$
EPAX [17] (pb)	0.06	1.5	1.8	69

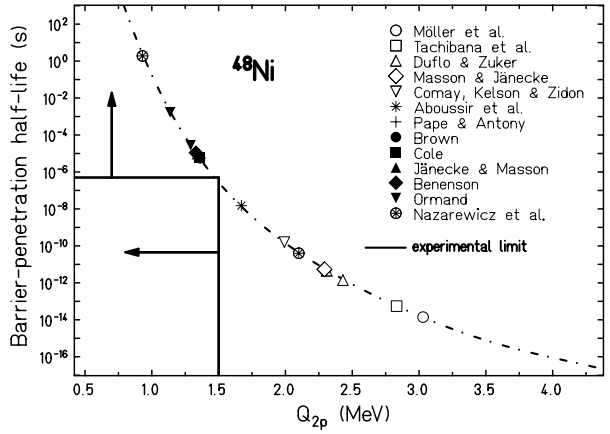

FIG. 3. Barrier-penetration half-life as a function of the two-proton Q value, Q_{2p}, for ^{48}Ni. The barrier penetration was calculated by assuming a spectroscopic factor of unity. Different model predictions [4–8,18–22] were used for Q_{2p}. The experimental observation of ^{48}Ni implies a half-life longer than 0.5 μs yielding an upper limit for Q_{2p} of about 1.5 MeV.

decay between 10^{-14} and 1 s. However, a closer inspection of the mass models used in Fig. 3 shows that "local models," i.e., models which either have been tailored to calculate masses in the region around ^{48}Ni [4–7] or which use local mass relations like the isobaric multiplet mass equation [18] or the Garvey-Kelson mass relation [19], predict Q_{2p} values which cluster at about 1.3 MeV. Some of the "global models" which consistently predict masses for a large part of the table of isotopes give also masses in this Q-value range [19]. However, most of them lie above 1.5 MeV and predict therefore much shorter half-lives. In microscopic calculations like those of Nazarewicz and coworkers [8], the masses depend on the Skyrme force used.

From the experimental observation of ^{48}Ni, we can deduce a limit of its half-life. Assuming that ^{49}Ni does not decay in flight, we can use the number of counts observed for this isotope to estimate the number of counts expected for ^{48}Ni. The transmissions for ^{48,49}Ni (see Table I) and a cross-section decrease of a factor of 26.4 $\pm$ 4.7 [12] allow us to deduce a number of counts expected for ^{48}Ni of 5.7 $\pm$ 2.2. With these figures and a total flight time of 1.32 μs, we obtain a half-life for ^{48}Ni of $2.6^{+\infty}_{-2.1}$ μs. We determine thus a lower limit at the 1σ level of 0.5 μs for the lifetime of ^{48}Ni. This value translates into an upper limit for Q_{2p} of about 1.5 MeV if we assume a spectroscopic factor of unity. Combined with the mass excess of 0.755 $\pm$ 0.354 MeV for ^{46}Fe [23], we determine therefore an upper limit for the mass excess of ^{48}Ni of 17.2 MeV. One should keep in mind that this determination is based on an extrapolated mass excess for ^{46}Fe and a spectroscopic factor of unity which make it only a rough estimate.

The β-decay half-life of ^{48}Ni is predicted to lie within a range of 5.9 to 11.3 ms [4,24]. Therefore, if the Q_{2p} value is, as predicted by several mass models, of the order of 1.3 MeV, which yields a barrier-penetration half-life of about 10^{-5} s, ^{48}Ni should decay by two-proton ground-state emission. Such a half-life should be accessible in future experiments.

In summary, we observed for the first time four events of the doubly magic nucleus ^{48}Ni. The experimental observation implies that its half-life is longer than about 0.5 μs. Using a spectroscopic factor of unity, this translates into an upper limit for Q_{2p} of 1.5 MeV. Several global mass models are in disagreement with this value, whereas local mass relations are in nice agreement with the present observations. Future measurements of the decay of ^{48}Ni which should be feasible after additional improvements of the primary-beam intensity should yield more detailed information on its mass and its decay properties.

We acknowledge the continuous effort of the GANIL accelerator staff to provide us with a stable, high-intensity beam. We express our sincere gratitude to the LISE staff for ensuring a smooth running of the LISE3 separator. This work was supported in part by the Polish Committee of Scientific Research under Grant No. KBN 2 P03B 036 15, the contract between IN2P3 and Poland, as well as by the Conseil Régional d'Aquitaine.

*Present address: Department of Physics and Astronomy, University of Tennessee, Knoxville, TN 37996-1200.

[1] R. Schneider *et al.,* Z. Phys. A **384**, 241 (1994).
[2] M. Lewitowicz *et al.,* Phys. Lett. B **332**, 20 (1994).
[3] C. Engelmann *et al.,* Z. Phys. A **352**, 351 (1995).
[4] B. A. Brown, Phys. Rev. C **43**, R1513 (1991).
[5] W. E. Ormand, Phys. Rev. C **53**, 214 (1996).
[6] W. E. Ormand, Phys. Rev. C **55**, 2407 (1997).
[7] B. J. Cole, Phys. Rev. C **54**, 1240 (1996).
[8] W. Nazarewicz *et al.,* Phys. Rev. C **53**, 740 (1996).
[9] F. Pougheon *et al.,* Z. Phys. A **327**, 17 (1987).
[10] A. C. Mueller and R. Anne, Nucl. Instrum. Methods Phys. Res., Sect. B **56**, 559 (1991).
[11] H. Geissel *et al.,* Nucl. Instrum. Methods Phys. Res., Sect. B **70**, 793 (1992).
[12] B. Blank *et al.,* Phys. Rev. C **50**, 2398 (1994).
[13] B. Blank *et al.,* Phys. Rev. Lett. **77**, 2893 (1996).
[14] D. Bazin, M. Lewitowicz, O. Sorlin, and O. Tarasov, simulation code LISE.
[15] B. Blank, E. Hanelt, and K.-H. Schmidt, simulation code LIESCHEN.
[16] J. Winger, B. Sherrill, and D. Morrissey, Nucl. Instrum. Methods Phys. Res., Sect. B **70**, 380 (1992).
[17] K. Sümmerer and B. Blank, Phys. Rev. C (to be published).
[18] W. Benenson, Nukleonika **20**, 775 (1975).
[19] P. E. Haustein (ed.), At. Data Nucl. Data Tables **39**, 185 (1988).
[20] P. Möller, J. R. Nix, W. D. Myers, and W. J. Swiatecki, At. Data Nucl. Data Tables **59**, 185 (1995).
[21] J. Duflo and A. P. Zuker, Phys. Rev. C **52**, R23 (1995).
[22] Y. Aboussir, J. Pearson, A. Dutta, and F. Tondeur, At. Data Nucl. Data Tables **61**, 127 (1995).
[23] G. Audi and A. H. Wapstra, Nucl. Phys. **A595**, 409 (1995).
[24] M. Hirsch, A. Staudt, K. Muto, and H. V. Klapdor-Kleingrothaus, At. Data Nucl. Data Tables **53**, 165 (1993).